Subject: paper
From: Christian Milea <chmilea@geo.auth.gr>
Date: Mon, 01 Feb 2010 11:26:50 +0200
To: kpapaza@geo.auth.gr

----- Προώθηση μηνύματος από c.gaffney@yahoo.co.uk -----
Ημερομ.: Thu, 28 Jan 2010 04:31:54 -0500 (EST)
Από: c.gaffney@yahoo.co.uk
Απάντησηc.gaffney@yahoo.co.uk
Θέμα: ARP-09-0038.R2 - Decision
Προς: chmilea@geo.auth.gr

28-Jan-2010

Dear Mr Milea,

It is a pleasure to accept your manuscript entitled "COMPLEX ATTRIBUTES OF THE MAGNETIC SIGNAL FOR MULTIPLE SOURCES: APPLICATION TO SIGNALS FROM BURIED DITCHES." in its current form for publication in Archaeological Prospection.

A signed Copyright Transfer Agreement (CTA) is needed for publication. If you have not already provided us with one you can access the CTA at:
http://media.wiley.com/assets/1540/86/ctaaglobal.pdf

If you have not yet uploaded a CTA, please ensure that you have identified the form with the manuscript ID number; scan your signed CTA and e-mail to cta@wiley.co.uk stating the manuscript ID number in the subject line of the e-mail.

If you do not have access to a scanner, please send your signed CTA to:

Wiley Services Singapore Pte Ltd,
600 North Bridge Road,
05-01 Parkview Square,
5188778, Singapore

Please note if the Contribution belongs to your employing institution, your employer should also sign the CTA.

If you have already provided us with the signed form, you do not need to do anything at this stage. You will be contacted by our typesetters/copyeditors shortly.

Thank you for your contribution.

Yours sincerely,

Dr Chris Gaffney
Archaeological Prospection
c.gaffney@yahoo.co.uk

----- Τέλος προωθημένου μηνύματος -----

Kwsta sou kanw forward thn apofash gia to paper. Epishs sou episunaptw to manuscript. An 8es tis eikones 8a tis valw sto LaCie me to pou mpaineis sto Christos(o fakelos mou), enas fakelos LAST. Gia oti allo 8eleis enhmerwse me

milea-cfg1_cor.doc	**Content-Type:** application/msword **Content-Encoding:** base64

COMPLEX ATTRIBUTES OF THE MAGNETIC SIGNAL FOR MULTIPLE SOURCES: APPLICATION TO SIGNALS FROM BURIED DITCHES.

Christian M. Milea[1], Richard O. Hansen[+2], Gregory N. Tsokas[1], Constantinos B. Papazachos[1] and Panagiotis I. Tsourlos[1].

[1] Exploration Geophysics Laboratory, School of Geology, Aristotle University of Thessaloniki, 54124 Thessaloniki, Greece

[2] Formerly at Pearson, deRidder and Johnson, Inc., 12860 W. Cedar Dr. Suite 102., Lakewood. Colorado 80228. U.S.A.

Abstract

Complex attributes of the magnetic signal are computed using a multiple source approach. Polygonal bodies are considered and the attributes of each corner are summed to produce the overall response; that is a decomposition of the polygonal body into magnetized steps to simulate the vertices. The method is tested on synthetic examples of buried ditches, as well as on real magnetic data. This type of target was selected because it comprises a common objective in "archaeological geophysics".

The resolution of the method in detecting the edges of the buried ditches depends on their lateral dimensions with respect to the sampling interval used. In general, the signal of the shallower most edges of the buried targets obscures the signal from the deeper corners thus prohibiting their detection. In some extreme cases, the signals from the deeper corners posed a recognizable signature. The analytic signal may be seen as an anomaly rectification technique. In this context, it is suitable for the presentation of "archaeological prospection" data since it provides an image

that resembles the plane view of the buried antiquities better than the total field anomaly itself.

Key words: Amplitude; Analytic signal; Complex attributes; Local wavenumber; Local Phase; Magnetic Prospection, Visualisation

1. Introduction

Magnetic prospecting comprises one of the main methods to locate and map buried antiquities. Subsurface remnants of old structures containing large amounts of burnt clay, such as kilns, are excellent targets because they usually show a strong magnetization contrast with respect to the medium they are hosted in. The method was also proved to be a powerful tool in mapping soil features, such as ditches, pits, trenches (Becker, 1995) or even tombs carved in magnetic environment (Piro et al. 2001). Further, the method is capable of mapping weakly magnetized buried remains of ancient structures such as ruins of foundation walls, etc.

It is well known that the treatment of the magnetic data presents difficulties due to the nature of the method itself. The magnetic anomalies are dipolar signals because of the dipolar nature of the magnetic fields created by magnetized bodies. The two lobes comprising the anomaly are asymmetrical and the center of the buried target is not located under the center of the anomaly. The quasi single lobe anomaly appears only in the case of vertical ambient field and vertical total magnetization of the target which should have also almost vertical dip. Furthermore extra trouble is added in magnetic prospection when the anomalies caused by buried structures are weak and superimposed.

For the reasons listed above, the interpretation of the magnetic anomalies shows an inherent difficulty. The problem is more pronounced for magnetic prospecting aiming to map buried antiquities than in any other application of the method. This is because the main targets are buried at the uppermost ground layers, which are usually heterogeneous and affected by modern cultural activity.

Regarding the asymmetry of the magnetic signal; the practitioners of the method were always seeking techniques that could eliminate it. Several techniques have been proposed to remove this asymmetry having various degrees of success. Reduction to the pole (Baranov 1957, Baranov and Naudy, 1964) removes the asymmetries caused by non- vertical magnetization, while pseudogravity (Baranov, 1957) transforms the dipolar field to monopolar vertical derivative. Space domain deconvolution of the magnetic anomalies (Tsokas et al., 1991; Tsokas and Papazachos, 1992; Tsokas, 1993) also leads to a better location of features. The technique of "terracing" (Cordel and McCafferty, 1989) can be also seen as operating in this direction. The aim is to transform the magnetic signal in a monopolar form which should be centered over the center of the buried target if possible. Therefore, the result of magnetic prospection, if presented as an image, could readily provide the impression of the plane view of the buried ruins (Scollar et al., 1986; Gaffney, 2009).

Regarding the resolution of nearby buried magnetic sources and possible extra information for the targets, the complex representation of the magnetic signal has been studied (Tsokas and Hansen, 1995, 2000; Blakely, 1995; Hsu et al. 1996; Tabbagh et al., 1997, Abas et al. 2005;Buyuksarac et al., 2008). It was shown that the analytic signal (the magnitude of the complex magnetic signal) possesses attractive geophysical and mathematical properties which make it very useful in archaeological prospection. The present paper extends the idea for multiple sources accounting thus,

for the corners of a horizontal body of polygonal section. It also investigates the exploitation of the technique in the search for buried ditches, which comprise a common target in "archeological geophysics". The performance of the analytic signal and the other complex attributes is studied along profiles of magnetic measurements over the particular targets. Synthetic data are produced by simulating several 2- D types of ditches using a custom built algorithm and computer code to solve the forward problem.

Nabighian (1972, 1974, 1984) proposed an interpretation method for magnetic data based on the concept of the analytic signal used in communication theory. This was extended by the introduction of complex attributes by Thurston and Smith (1997), Thurston et al. (2002) and Smith et al. (1998). The analytic signal method applies for 2D bodies and assumes: a) a uniform magnetization of the considered bodies, b) that these bodies are limited by planar faces. The mathematical and geophysical properties of the analytic signal are much more attractive in archaeological prospection where the buried targets usually have geometrical shapes. Its amplitude, as well as the local wavenumber function (as will be shown later), peak exactly over the edge of a dipping contact, suggesting that they can both be used to show peaks above every corner of a buried target. Also, all the complex attributes functions (amplitude, local phase, local wavenumber) are independent of the inclination, declination and remanent magnetization for the 2- D sources (Blakely, 1995:351; Thurston and Smith, 1997).

2. The complex attributes

The analytic signal is defined as

$$A(x) = T(x) - T_1(x) \ , \tag{1}$$

where $T_1(x)$ is the Hilbert transform of the real function T(x). Nabighian (1972) showed that the horizontal derivative $\partial M/\partial x$ and the vertical derivative $\partial M/\partial z$ of a magnetic anomaly M form a Hilbert transform pair and for contact at depth h and dipping at an angle d is given by the equations

$$T(x) = \frac{\partial M(x)}{\partial x} = 2kFc \cdot \sin d \, \frac{(h-z)\cos\phi + x\sin\phi}{(h-z)^2 + x^2} \tag{2}$$

and

$$T_1(x) = \frac{\partial M(x)}{\partial z} = 2kFc \cdot \sin d \, \frac{x\cos\phi - (h-z)\sin\phi}{(h-z)^2 + x^2} \tag{3}$$

respectively (Nabighian, 1972), where

k is the susceptibility contrast of the step,

F is the earth's magnetic field,

c and φ are constants that for total field anomaly take the forms $c=1-\cos^2 i \sin^2 A$ and $\varphi = 2I - d - 90$ (in this paper we deal only with total field anomalies),

i is the geomagnetic field's inclination, d is the dip angle of the contact and h the burial depth.

A is the angle between the magnetic north and the positive x axis (azimuth),

I is given by the relation $\tan I = \tan i / \cos A$.

In equation (2) and (3) the anomaly M is considered only as a function of the x variable (along the profile) since measurements are usually obtained on a constant height z (for instance 0.5 m above the ground), which is usually the case in archaeological prospection.

For the complex function of the analytic signal A(x) we can get three real functions, the amplitude, the phase and the wavenumber. It follows from equations (2)

and (3), that the amplitude, phase and wavenumber of the analytic signal of a contact dipping at an angle d and at depth h, are given by the equations

$$|A(x)| = \sqrt{\left(\frac{\partial M}{\partial x}\right)^2 + \left(\frac{\partial M}{\partial z}\right)^2} = \frac{a}{\left[(h-z)^2 + x^2\right]^{1/2}} \quad , \tag{4}$$

$$\theta = \tan^{-1}\left[\frac{\partial M}{\partial z} \Big/ \frac{\partial M}{\partial x}\right] = \tan^{-1}\left(\frac{x\cos\phi - (h-z)\sin\phi}{(h-z)\cos\phi + x\sin\phi}\right) \tag{5}$$

and

$$k = \frac{1}{|A(x)|^2}\left(\frac{\partial^2 M}{\partial x \partial z}\frac{\partial M}{\partial x} - \frac{\partial^2 M}{\partial x^2}\frac{\partial M}{\partial z}\right) = \frac{h-z}{(h-z)^2 + x^2} \tag{6}$$

respectively (Thurston and Smith, 1997), where *a=2kFcsind*. The functions of the amplitude, the phase and the wavenumber are called complex attributes of the analytic signal.

3. Calculating the Complex attributes for a polygonal body

The equations presented in the previous paragraph estimate the complex attributes of the magnetic signal for a single dipping 2D contact. However, this is not usually the case in archaeological prospection where the targets are buried volumes, which can be usually simulated quite accurately with polygonal bodies. Therefore, any attempt to simulate these targets should take into account the set of the corners (finite steps) that constitute the body.

Our calculations concern total field magnetic anomalies. The total field **T** in a point, due to the regional earth's magnetic field **F** and the anomaly **ΔF** caused by a magnetized body is

$$\mathbf{T} = \mathbf{F} + \Delta\mathbf{F} \quad , \tag{7}$$

where the bold letters indicate vectors. The magnitude of the total field is given by

$$\left|\mathbf{T}\right| = \left|\mathbf{F} + \Delta\mathbf{F}\right| \approx \left|\mathbf{F}\right| + \mathbf{f} \cdot \Delta\mathbf{F} \quad , \tag{8}$$

$\mathbf{f}$ being the unit vector along the regional field. The quantity $\left|\mathbf{T}\right|$ is what the total field magnetometers measure. Equation (8) holds when the anomalous field is much smaller than the regional field, $\Delta\boldsymbol{F} << \boldsymbol{F}$, and when the regional field's direction is constant through the survey area. Both conditions are practically satisfied in archaeological prospection (Blakely, 1995).

For a body of polygonal section, the anomaly that it produces consists of the sum of the anomalies produced by each side. The total field anomaly caused by the polygonal body having n corners (or sides), is then

$$M = \mathbf{f} \cdot \sum_{i}^{n} \Delta\mathbf{F}_i = \sum_{i}^{n} \mathbf{f} \cdot \Delta\mathbf{F}_i = \sum_{i=1}^{n} M_i =$$

$$= \sum_{i=1}^{n} \left\{ 2kFc \sin d_i \cdot \left[\left(\theta_1^i - \theta_2^i \right) \cdot \cos\phi_i + \sin\phi_i \ln \frac{r_1^i}{r_2^i} \right] \right\} \quad . \tag{9}$$

The meaning of θ_1, θ_2, r_1 and r_2 can be seen in Figure 1. The side is equivalent to a finite step and the anomaly of the whole body is obtained by adding and substracting accordingly the effect of four finite steps for the case of Figure 1.

This consideration implies that the principle of superposition applies for our case. Therefore, we assume that the magnetic field from each side only slightly affects its neighboring ones, so as to produce very small induced magnetization, which is practically zero.

Any polygonal two- dimensional body can be obtained by superimposing a finite number of magnetized steps. Consequently the magnetized body $\overline{ABCD}$ of Figure 1 is given by (Nabighian 1972):

$$\overline{ABCD} = \overline{ADEF} + \overline{BAFH} - \overline{BCGH} - \overline{CDEG} \quad . \tag{10}$$

For this case, a positive sign is assigned to the sides AB and AD and negative for the BC and CD ones. However, it is necessary to determine the sign of the anomaly of each polygon side automatically, hence, we followed the Talwani and Heirtzler's (1964) convention. According to this convention, if we are proceeding in a clockwise direction along the polygon, a positive sign in relation (9) emerges for sides whose angle θ increases (i.e $\theta_2 > \theta_1$).

For the calculation of complex attributes (amplitude, phase and wavenumber) relationships (2) to (6) are used. We should note that relationships (2) and (3) (hence (4), (5) and (6)) do not refer to a finite magnetized step (side of the polygon), but to a contact (corner of the polygon, i.e infinite step). This means that for the calculation of the complex attributes of a polygonal body we refer to the corners of a side and not to the side itself, as it happens when calculating the magnetic anomaly.

A finite magnetized step can be obtained by superimposing two magnetized contacts of infinite depth and opposite polarity. Therefore the magnetic anomaly caused by the Figure's 2 quadrangle ABCD can be obtained by superimposing 8

contacts whose depth extends to infinity, forming couples corresponding to the same side. Thus,

$$\overline{ABCD} = \left(\overline{ED1} + \overline{FA1} + \overline{GC2} + \overline{ED2}\right) - \left(\overline{FA2} + \overline{HB1} + \overline{HB2} + \overline{GC1}\right) \quad . \qquad (11)$$

The real and imaginary part of the analytic signal of an N- sided polygonal magnetized body is

$$\bullet\ \mathrm{T}(\mathrm{x}) = \frac{\partial \mathrm{M}}{\partial \mathrm{x}} = \mathrm{a}\sum_{\mathrm{k}=1}^{\mathrm{N}}\left[\sin \mathrm{d}^{\mathrm{k}}\,\frac{(\mathrm{x}-\mathrm{x}_{\mathrm{k}})\sin\phi_2^{\mathrm{k}} + (\mathrm{z}_{\mathrm{k}}-\mathrm{z})\cos\phi_2^{\mathrm{k}}}{(\mathrm{z}_{\mathrm{k}}-\mathrm{z})^2 + (\mathrm{x}-\mathrm{x}_{\mathrm{k}})^2} - \right.$$
$$\left. - \sin \mathrm{d}^{\mathrm{k}}\,\frac{(\mathrm{x}-\mathrm{x}_{\mathrm{k}})\sin\phi_1^{\mathrm{k}} + (\mathrm{z}_{\mathrm{k}}-\mathrm{z})\cos\phi_1^{\mathrm{k}}}{(\mathrm{z}_{\mathrm{k}}-\mathrm{z})^2 + (\mathrm{x}-\mathrm{x}_{\mathrm{k}})^2}\right] \qquad (12)$$

and

$$\bullet\ \mathrm{T}_1(\mathrm{x}) = \frac{\partial \mathrm{M}}{\partial \mathrm{z}} = \mathrm{a}\sum_{\mathrm{k}=1}^{\mathrm{N}}\left[\sin \mathrm{d}^{\mathrm{k}}\,\frac{(\mathrm{x}-\mathrm{x}_{\mathrm{k}})\cos\phi_2^{\mathrm{k}} - (\mathrm{z}_{\mathrm{k}}-\mathrm{z})\sin\phi_2^{\mathrm{k}}}{(\mathrm{z}_{\mathrm{k}}-\mathrm{z})^2 + (\mathrm{x}-\mathrm{x}_{\mathrm{k}})^2} - \right.$$
$$\left. - \sin \mathrm{d}^{\mathrm{k}}\,\frac{(\mathrm{x}-\mathrm{x}_{\mathrm{k}})\cos\phi_1^{\mathrm{k}} - (\mathrm{z}_{\mathrm{k}}-\mathrm{z})\sin\phi_1^{\mathrm{k}}}{(\mathrm{z}_{\mathrm{k}}-\mathrm{z})^2 + (\mathrm{x}-\mathrm{x}_{\mathrm{k}})^2}\right]$$

respectively. The amplitude and the phase are respectively

$$\mathrm{A}(\mathrm{x}) = \sqrt{\mathrm{T}^2(\mathrm{x}) + \mathrm{T}_1^2(\mathrm{x})} = \mathrm{a}\cdot\left\{\left(\sum_{\mathrm{k}=1}^{\mathrm{N}}\left[\sin \mathrm{d}^{\mathrm{k}}\,\frac{(\mathrm{x}-\mathrm{x}_{\mathrm{k}})\sin\phi_2^{\mathrm{k}} + (\mathrm{z}_{\mathrm{k}}-\mathrm{z})\cos\phi_2^{\mathrm{k}}}{(\mathrm{z}_{\mathrm{k}}-\mathrm{z})^2 + (\mathrm{x}-\mathrm{x}_{\mathrm{k}})^2} - \right.\right.\right.$$
$$\left.\left.\left. - \sin \mathrm{d}^{\mathrm{k}}\,\frac{(\mathrm{x}-\mathrm{x}_{\mathrm{k}})\sin\phi_1^{\mathrm{k}} + (\mathrm{z}_{\mathrm{k}}-\mathrm{z})\cos\phi_1^{\mathrm{k}}}{(\mathrm{z}_{\mathrm{k}}-\mathrm{z})^2 + (\mathrm{x}-\mathrm{x}_{\mathrm{k}})^2}\right]\right)^2 + \right.$$
$$\left. + \left(\sum_{\mathrm{k}=1}^{\mathrm{N}}\left[\sin \mathrm{d}^{\mathrm{k}}\,\frac{(\mathrm{x}-\mathrm{x}_{\mathrm{k}})\cos\phi_2^{\mathrm{k}} - (\mathrm{z}_{\mathrm{k}}-\mathrm{z})\sin\phi_2^{\mathrm{k}}}{(\mathrm{z}_{\mathrm{k}}-\mathrm{z})^2 + (\mathrm{x}-\mathrm{x}_{\mathrm{k}})^2} - \right.\right.\right.$$
$$\left.\left.\left. - \sin \mathrm{d}^{\mathrm{k}}\,\frac{(\mathrm{x}-\mathrm{x}_{\mathrm{k}})\cos\phi_1^{\mathrm{k}} - (\mathrm{z}_{\mathrm{k}}-\mathrm{z})\sin\phi_1^{\mathrm{k}}}{(\mathrm{z}_{\mathrm{k}}-\mathrm{z})^2 + (\mathrm{x}-\mathrm{x}_{\mathrm{k}})^2}\right]\right)^2\right\} \qquad (13)$$

and

$$\theta(x) = \tan^{-1}\frac{T_1(x)}{T(x)} \quad . \qquad (14)$$

In relationship (13) the functions *T(x)* και *T1(x)* are given by equations (12). In equation (4) the constant α was defined as *a=2kFcsind*, whereas in the above relationships it is *a=2kFc* (which we adopt throughout the end of this paper), since the dip d is different for each side of the polygon.

For the wavenumber's calculation we need the second derivatives $\frac{\partial^2 M}{\partial x^2}$ and $\frac{\partial^2 M}{\partial x \partial z}$, which is easily shown to be given from the equations

$$\begin{aligned} \bullet\ & \frac{\partial^2 M^k}{\partial x \partial z} = \frac{\partial}{\partial x}\left(\frac{\partial M^k}{\partial z}\right) = \frac{-2(x - x_k)\cdot T^k{}_1(x) + a\cdot(\sin d^k \cos\phi_2^k - \sin d^k \cos\phi_1^k)}{(z_k - z)^2 + (x - x_k)^2} \\ \bullet\ & \frac{\partial^2 M^k}{\partial x^2} = \frac{\partial}{\partial x}\left(\frac{\partial M^k}{\partial x}\right) = \frac{-2(x - x_k)\cdot T^k(x) + a\cdot(\sin d^k \sin\phi_2^k - \sin d^k \sin\phi_1^k)}{(z_k - z)^2 + (x - x_k)^2} \end{aligned} \qquad (15)$$

for the k- th angle of the polygon. Therefore the wavenumber is

$$\begin{aligned} k(x) = \frac{1}{|A|^2}\cdot\Bigg\{ & \left[\sum_{k=1}^{N} \frac{-2(x - x_{k)}\cdot T^k{}_1(x) + a\cdot(\sin d^k \cos\phi_2^k - \sin d^k \cos\phi_1^k)}{(z_k - z)^2 + (x - x_k)^2}\right]\cdot T(x) - \\ & - \left[\sum_{k=1}^{N} \frac{-2(x - x_{k)}\cdot T^k(x) + a\cdot(\sin d^k \sin\phi_2^k - \sin d^k \sin\phi_1^k)}{(z_k - z)^2 + (x - x_k)^2}\right]\cdot T_1(x)\Bigg\} \end{aligned} \qquad (16)$$

The formulation previously described can be easily applied for any polygonal body. First the dip of each side is calculated and the magnetic anomaly is computed from equation (9). The real $T^i(x)$ and imaginary part $T_1{}^i(x)$ of the analytic signal are then calculated, using equations (11) and (12) (equation (12) is adapted according to the number of the body's sides). Thereafter, we use Talwani and Heirtzler's

convention, to define the signs for each term of equation (12), and then the complex attributes are calculated.

4. Complex attributes of anomalies produced by buried ditches

An appropriate computer code has been developed to calculate the magnetic anomaly and the complex attributes of 6 simple models of various types of ditches (Fig. 3). The model shown at the top of Figure 3 (a) simulate a rectangular shape, while triangular shapes are shown next (b and c). A scalene (scalene is a triangular having uneven all sides - Fig3c) and an isosceles triangle were chosen. The three next models (d, e and f) represent heptagonal ditches. The last models were considered because they are good approximations of semi cylindrical ditches. Various other models were considered in the framework of the present study but these calculations are not presented here because the length of the paper would have increased enormously.

The rectangular model can be considered as representing not only a ditch but also any rectangular buried structure. The geometrical parameters for the measuring transect and the elements of the ambient field are identical for all calculations. The profile's length was assessed to 20 m and the sampling interval set 0.5 m (both these numbers are commonly used in archaeological prospection). The Earth's magnetic field was set to 46000 nT, the inclination to 55^0 and the azimuth 0^0, while .the susceptibility contrast between the bodies and the surrounding medium was put as 0.005 SI units.

The magnetic anomaly, its horizontal and vertical derivative, as well as its complex attributes (amplitude, phase and wavenumber), for a thin rectangular

magnetized ditch (or body) are shown in Figure 4. The ditch is 2 m wide and 0.5 m deep, buried at 0.5 m depth (model a in Figure 3).

The results presented in Figure (4) show that the maxima of the amplitude and the vertical derivative occur exactly over the edges of the buried body. The position of the edges also coincides with the points where the horizontal derivative becomes zero. The maxima of the amplitude are very close, as a result of the particular sampling interval (0.5 m) and the relatively small horizontal dimension of the body (2 m). However, the peaks are discernible.

It is evident from Figure 4 that the local wavenumber and the local phase detect the edges of the body quite well, showing maxima and discontinuities respectively, at the relevant positions. It should be noted that the signals of the deep corners, and therefore any function computed from that signals, are “hidden”, as they are located exactly under the shallower ones.

The response of two models simulating ditches of triangular shape (models b and c in Figure 3) was studied next. Specifically, a body having the shape of an inverted scalene triangle, of base 6 m and high 0.5 m, and another isosceles triangular body of dimensions, 3×2 were studied. The same quantities as for the rectangular shape were computed and are shown in Figures 5 and 6.

Regarding the magnetic anomaly, the spatial derivatives and the phase similar conclusions to those for the rectangular bodies can be inferred. For the last case, i.e. that where the lateral dimension of the target is small, the local phase shows its powerful resolving ability since the edges of the ditch are pretty well located. However, the method fails in both cases to detect the top of the triangles, i.e. the corner that lies deeper.

The local amplitude and wavenumber responses of the wide ditch (Fig. 5) show some very interesting features. The local wavenumber provides some hint for the deepest corner. Of course this is a noise free calculation and therefore it is evident that its detection would be rather difficult in real data. Further, regarding the local amplitude, its graph is diagnostic for the existence of the deep corner (top of the triangle) only in the case of the scalene triangle, which, on the other hand, is shallower than that of the isosceles triangle. This behavior was more or less expected, since the amplitude function has a smaller fall off rate than the wavenumber.

For the relatively narrower target (Fig. 6), both the local amplitude and wavenumber lose their resolving ability and fail to discriminate the corners of the base of the triangles.

To summarize, the local phase function is fully diagnostic for locating the edges in all cases while the other complex attributes provide limited information. The presence of the top of the triangle cannot be inferred safely by any one of the complex attributes.

The various anomalies produced by the last three heptagonal models (models d,e and f in Figure 3) can be seen in Figures 7 to 9. Two large bodies, a heptagon of dimensions 12 m × 3 m is presented in Figure 7. On the other hand, two smaller heptagonal bodies, of dimensions 3 m × 1.5 m and 1 m × 0.5 m, are shown, respectively, in Figure 8 and 9.

Concerning the widest model, it can be seen in Figure 7 that all attributes locate the outer corners and but none of the others. However, the wavenumber provides some hint on the existence of the deepest corner. Displacement with respect to the corners' locations of the maxima (and discontinuities) of all attributes are also observed, due to the sampling spacing but also reflecting the superposition of the

signal of the shallower corners. The displacement is particularly evident in the phase curve; the discontinuity in the left edge is moved towards right. However, all displacements are very small and they can be considered negligible within the locating accuracy provided by the sampling interval used.

Similar conclusions are drawn from the model of Figure 8. For this case, no indication of any deep corner is provided and all attributes peak only at the edge corners. The model is thinner than that in the previous case but still the edge corners are located by all attributes, being clearly discernible except in the amplitude. Note that the phase curve shows an unambiguous accuracy in locating the bodies' edges.

In Figure 9 it is seen that both the amplitude and the wavenumber lose their resolving abilities to detect the body's edges (only one peak is seen), due to the very small dimensions of the body. However, the phase manages to locate both edges with great accuracy.

5. Application to the magnetic data over the prehistoric site of Makrygialos in Northern Greece.

The method of complex attributes was applied in real total field magnetic data. The data set used was taken from a large- scale magnetic survey that was conducted by Tsokas et. all (1997) in the archaeological area of Makrygialos, in Pieria, (Region of Macedonia, Northern Greece). The area of Makrygialos constitutes one of the most active regions in Greece in terms of archaeological excavations that have taken place over the last 30 years.

A particular bit of data was selected for the demonstration of the present paper consisting of one 40mX40m grid whose conventional name is 024. Data were collected along traverses spaced 1 m apart each from the other stepwise at 1 m intervals. The measuring mode renders the survey as low resolution. The measured

total field magnetic data of the grid 024 have undergone conventional processing including despiking, edge match and low pass filtering. The resulting distribution of the magnetic field magnitude is shown in Figure 10. Two pronounced magnetic anomalies are observed ranging almost perpendicular to the North – South axis at its 7th and 25th metre. These anomalies were conventionally named as 1 and 2 and they reflect the presence of concealed prehistoric ditches unearthed in a nearby location. Complex attributes for multiple sources were computed along two NS ranging profiles, shown in Figure 10 as profile1 and profile2, which cut the horizontal axis at 5 m and 18 m respectively.

The calculated functions of the amplitude, horizontal and vertical derivatives, wavenumber and phase for each profile are shown in Figures 11 and 12 respectively. Noise is affecting the results and combined with the low resolution of the survey (1 m sampling interval) reduces the detecting ability of the wavenumber curve and eliminates that of the phase curve. This is due to the sensitivity at noise of the second derivatives used in the computation of both wavenumber and phase. Further, the sampling interval (1 m) adds more noise to the numerical differentiations. Another source of instability is raised because the wavenumber and phase are computed after calculating the amplitude and taking into account its numerical value. Therefore, any error in the computation of the amplitude is amplified into the next computations.

However the amplitude curve manages to locate exactly the two ditches, which create clear maxima along both profiles. Figure 13 shows the distribution of the amplitude over the 40mX40m grid, obtained by applying the technique of complex attributes of multiple sources over the whole grid. The anomalies produced by the ditches can be seen as rectified versions of the total filed anomalies centered over the centers of the buried bodies.

6. Conclusions

Both the magnetic anomaly's derivatives (horizontal and vertical) located satisfactorily the edges of the bodies in all cases, but without detecting any mediate corners. This is well known and more or less expected but was also inferred from the multiple sources approach followed in this paper. This is mainly due to the fact that the signal of lower corners is obscured by that of the upper ones, in combination with the decrease of the signal strength with depth.

The analytic signal's resolving ability depends on the bodies' dimensions. For targets having lateral dimension less than 3 m, the peaks of the maxima are very close and there can be difficultly in discerning edges in real situations. When the corners are as close as four sampling intervals (one spacing unit is 0.5 m for the synthetic examples demonstrated) then the peaks of the maxima practically merge so that only one peak appears. Also when the mediate corners are too close with respect to the shallower (outer) ones, there is a complete overlap of the peaks they produce with that of the shallow corners. The case of the synthetic inverted triangles showed that the analytic signal of the deep corners (top of triangles) can be differentiated only if the horizontal distance is sufficient. Indeed, this is a noise free consideration, which means that signal from the top of the triangles will be hardly recognized in real cases.

Similar conclusions can be inferred for the wavenumber function. If the target has lateral dimension twice the sampling interval (0.5 m – Fig. 13), the shallow edge corners response merge into one peak. The wavenumber function has a smaller fall off rate than the analytic signal and therefore the response of the mediate corners show up better, provided that their burial depth is not big (Figs 5,6 and 7). Due to the same reason, the response of the shallower corners is more discernible for the wavenumber.

This is evident in all the synthetic examples considered, except the case of the thin heptangular body (Fig. 13) whose lateral extent is two sampling intervals. In general, the wavenumber peaks are very clear and distinguishable. Therefore, the wavenumber is much more capable in locating the edges of buried bodies, preserving its resolution ability even for small bodies, in contradiction with the behavior of the analytic signal.

The phase managed to detect the edges of the buried bodies in all synthetic examples, but also failed to locate the intermediate corners in anyone of them. Furthermore, for large lateral dimension of the buried bodies (greater than 5 m), the discontinuities of the phase curve are slightly displaced towards the center of the bodies.

It should be noted that the analytic signal rectified the anomalies seen in the total field anomaly map. The locations and shapes of the anomalies were in excellent agreement with the plane view of the buried targets (projection of the body on the ground surface). This outcome shows that complex attributes can be efficiently used for transforming the data in a form which is more suitable for the final presentation of the results of an archaeological prospection survey. Although wavenumber and phase are very sensitive to noise, they can be combined with other functions, such as analytic signal and the spatial derivatives, or any other type of information, to infer conclusions for the buried bodies.

Application of the method to real data showed that it is highly influenced by noise, in particular regarding the local wavenumber and phase curves. Noise highly affects the second derivative computation and also any numerical differentiation involved. The low resolution character of the example makes the situation worse, rendering the wavenumber and phase curves as useless for the particular case.

However, the amplitude curve (amplitude of analytic signal) successfully transformed the data into a monopolar form centered over the disturbing buried structures.

The observed instability of the local phase and wavenumber due to data noise and spatial sampling shows that additional work needs to be done in order to evaluate their efficient use for similar studies which is the subject of ongoing research work.

REFERENCES

Abas M.A., T.F. Abdallatif, F.A. Shaaban, A. Salem, and M. Suh, 2005, Archaeological investigations of the eastern extentions of the Karnak Temple using Ground – Penetrating Radar and magnetic tools: Geoarchaeology, **20**, 5, 537-554.

Baranov V., 1957, A new method for interpretation of aeromagnetic maps: pseudo-gravimetric anomalies: Geophysics, **22**, 359- 383.

Baranov V., and H. Naudy, 1964, Numerical calculation of the formula of reduction to the magnetic pole: Geophysics, **29**, 67- 79.

Becker H., 1995, From nanotesla to picotesla - a new window for magnetic prospecting in Archaeology: Archaeological Prospection, **2**, 217- 228.

Blakely R.J., 1995, Potential theory in gravity and magnetic applications: Cambridge University Press, New York.

Büyüksaraç A., M. Ö. Arisoy, Ö. Bektaş, Ö. Koçak, and T. Çay, 2008, Determination of Grave Locations in Dedemezari Necropolis (Western Turkey) using Magnetic Field Derivatives: Archaeological Prospection, **15,** 267-283.

Cordell L., and A. E. McCafferty, 1989**,** A terracing operator for physical property mapping with potential field data: Geophysics, **54**, 621-34.

Gaffney, C. 2009, The use of geophysical techniques in landscape studies: experience from commercial sector: In Seeing the Unseen. Geophysics and Landscape Archaeology, edited by S. Campana and S. Piro, ISBN 978-00415-44721-8, Taylor and Francis Group, 201-206.

Hsu S.K., Sibuet J.C., and Shyu C.T., 1996, High – resolution detection of geologic boundaries from potential anomalies:An enhanced analytic signal technique: Geophysics, **61**, 373-386.

Nabighian M. N., 1972, The analytic signal of two- dimensional magnetic bodies with polygonal cross- section: Its properties and use for automated anomaly interpretation: Geophysics, **37**, 507- 517**.**

Nabighian M. N., 1974, Additional comments on the analytic signal of two-dimensional magnetic bodies with polygonal cross- section: Geophysics, **39**, 85-92**.**

Nabighian M. N., 1984, Toward a three- dimensional automatic interpretation of potential field via generalized Hilbert transforms: Fundamental relations: Geophysics, **49**, 780-6**.**

Piro S., P.I. Tsourlos, and G. N. Tsokas, 2001, Cavity detection employing advanced geophysical techniques: a case study: European Journal of Environmental and Engineering Geophysics, **6**, 3-31.

Scollar I., B. Weidner, and K. Segeth, 1986, Display of archaeological magnetic data: Geophysics, **51**, 623-633.

Smith R. S., J. B. Thurston, D. T. Fan, and I. N. MacLeod, 1998, iSPI™- the improved source parameter imaging method: Geophysical Prospecting, **46**, 141-151.

Tabbagh A., G. Desvignes, and M. Dabas, 1997, Processing of Z gradiometer magnetic data using linear transforms and analytic signal: Archaeological Prospection, **4 (1)**, 1-13.

Talwani M., and J.R. Heirtzler, 1964, Computation of magnetic anomalies caused by two dimensional structures of arbitrary shape: Stanford University Publications.

Thurston J. B., and R.S. Smith, 1997, Automatic conversion of magnetic data to depth, dip and susceptibility contrast using the SPI (TM) method: Geophysics, **62 (3)**, 807- 813.

Thurston J. B., R. S. Smith, and J. C. Guillon, 2002, A multimodel method for depth estimation from magnetic data: Geophysics, **67**, 555- 561.

Tsokas G. N., 1993**,** An investigation of the effectiveness of inverse filtering in the geophysical search of archaeological sites: Theory and practice of applied geophysics, **7**, Geophysical Exploration of Archaeological Sites, Vogel and Tsokas eds: 72-88.

Tsokas G. N., and C. B. Papazachos, 1992, Two- Dimensional Inversion Filters in Magnetic Prospecting: Application to the Exploration for Burried Antiquities: Geophysics, **57**, 1004- 1013.

Tsokas G.N., and R.O. Hansen, 1995, A comparison of inverse filtering and multiple source Werner deconvolution for model archaeological problems: Archaeometry, **37**, 1, 185-193.

Tsokas G.N., and R. O. Hansen, 2000, On the use of complex attributes and the inferred source parameter estimates in the exploration of archaeological sites: Archaeological Prospection, **7,** 1, 17-30.

Tsokas G. N., C. B. Papazachos , M. Z. Loucoyannakis, and O. Karousova, 1991, Geophysical data from archaeological sites: Inversion filters based on the vertical-sited finite prism model: Archaeometry **33**, 215- 230.

Tsokas G.N., Pappa M., Bessios M., Papazachos C.B., Tsourlos P., and Giannopoulos A., 1997, A large scale magnetic survey in Makrygialos (Pieria), Greece: Archaeological Prospection, **4,** 123-137.

FIGURES

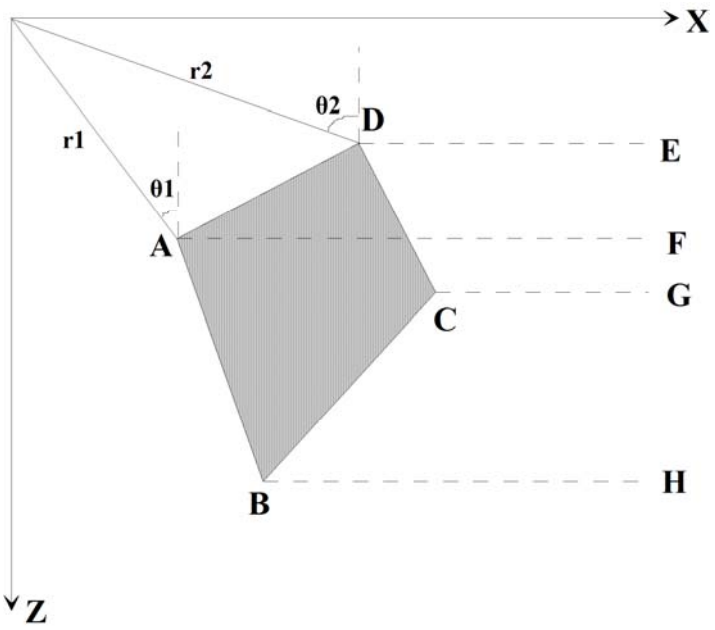

Figure 1*: Cross- section of a magnetized polygonal body decomposed in 4 magnetized finite steps.*

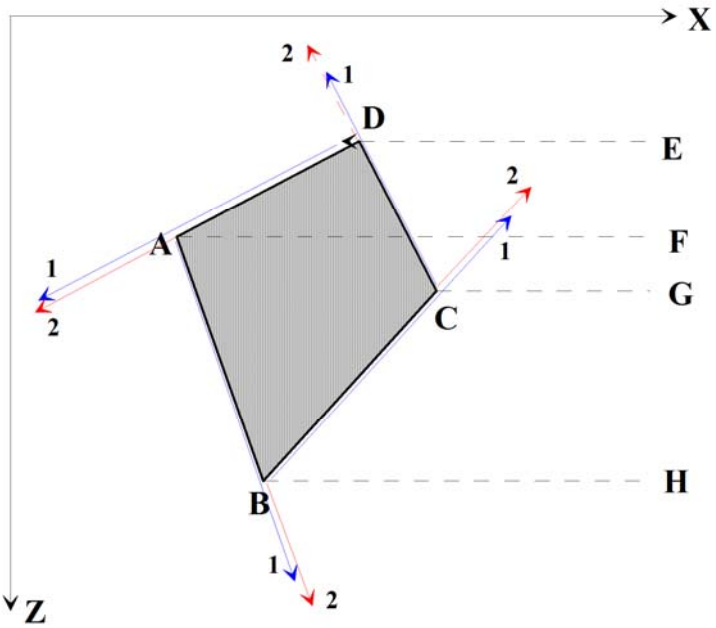

Figure 2*: Magnetized quadrangle that results by the superposition of 8 infinite steps (contacts).*

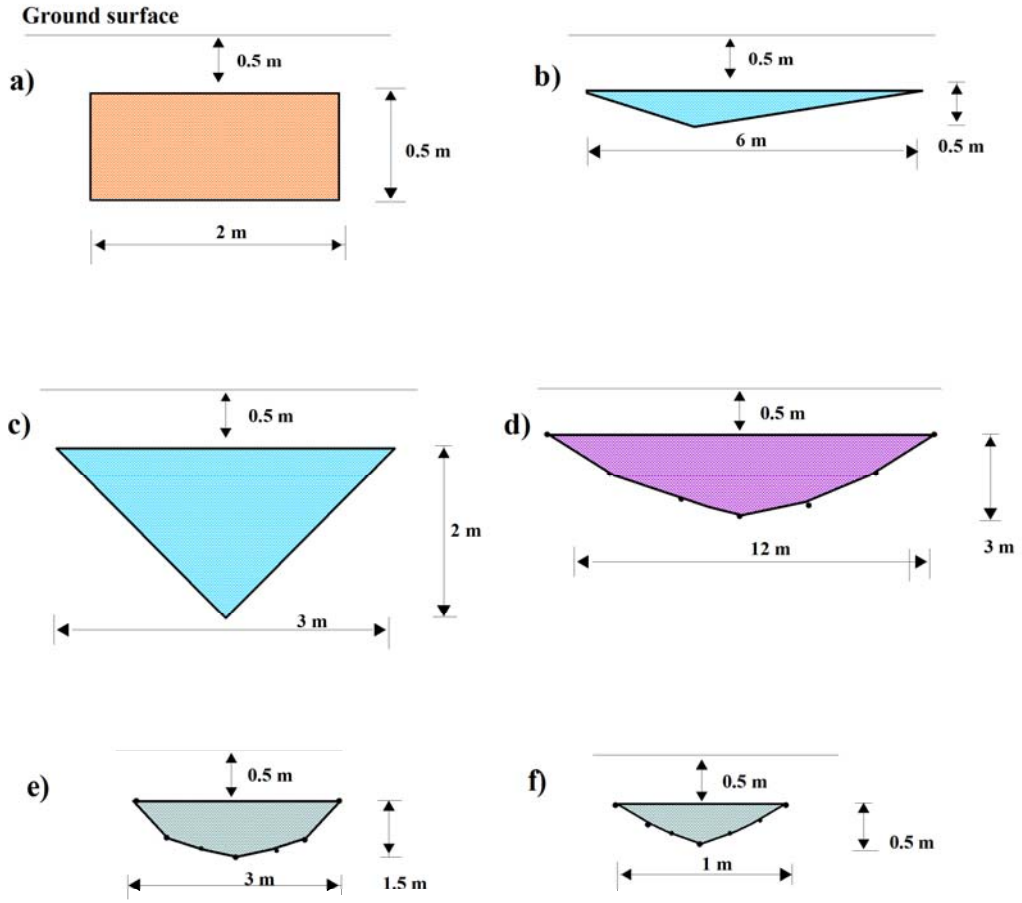

***Figure 3**: The models used for the simulations.*

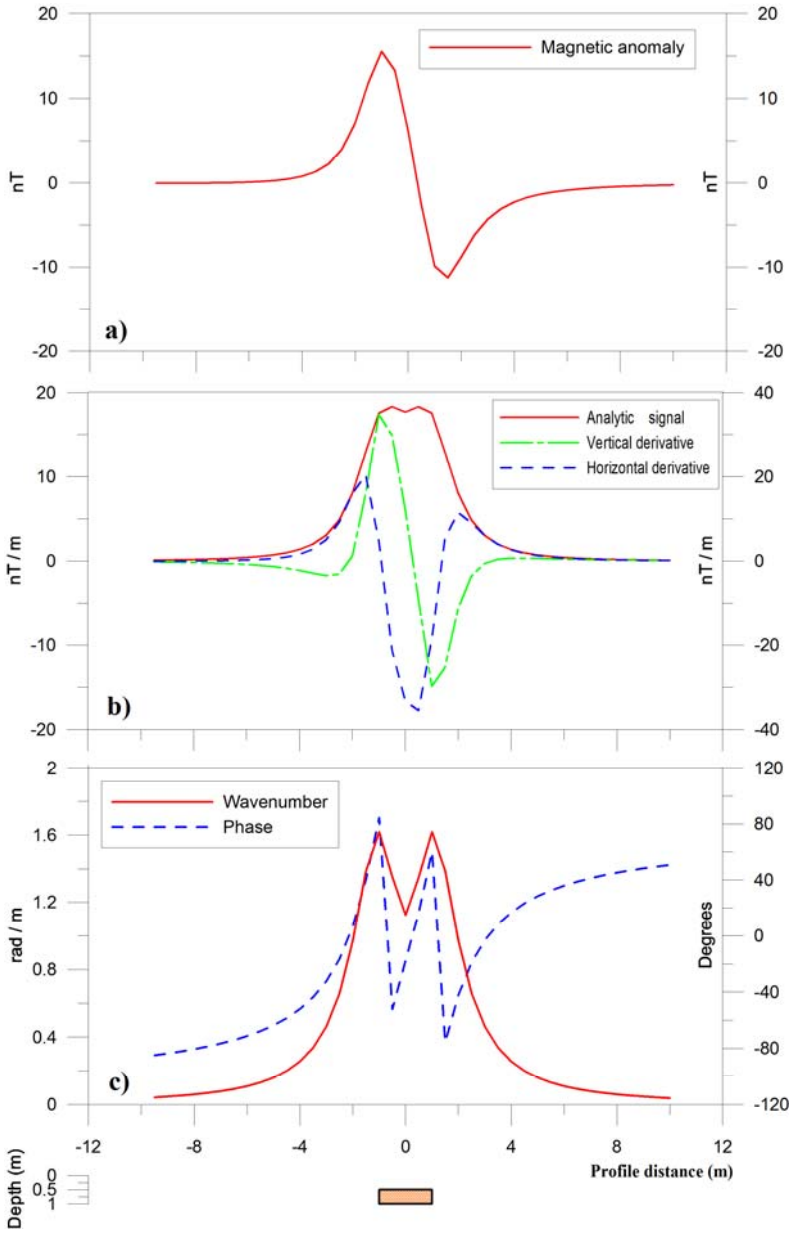

Figure 4*: A rectangular body of dimensions 2 m× 0.5 m (model a in Figure 3) is shown at the bottom of the figure. The magnetic anomaly that it produces is in (a) and the horizontal and vertical derivative and the analytic signal is in (b). The local phase and the local wavenumber are shown in (c).*

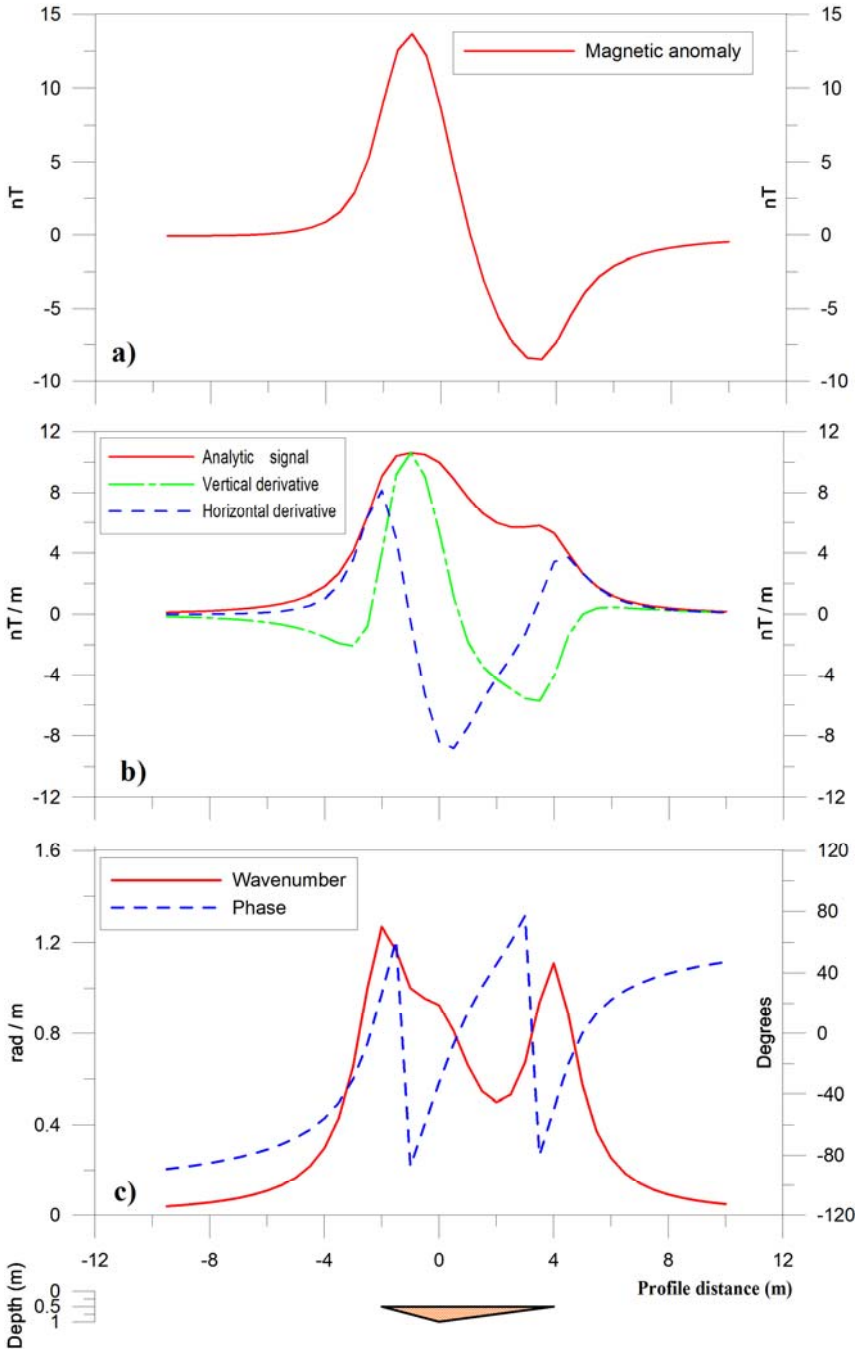

Figure* 5: Same as Figure (4) for the triangular body of dimensions 6 m × 0.5 m (model b of Figure 3).*

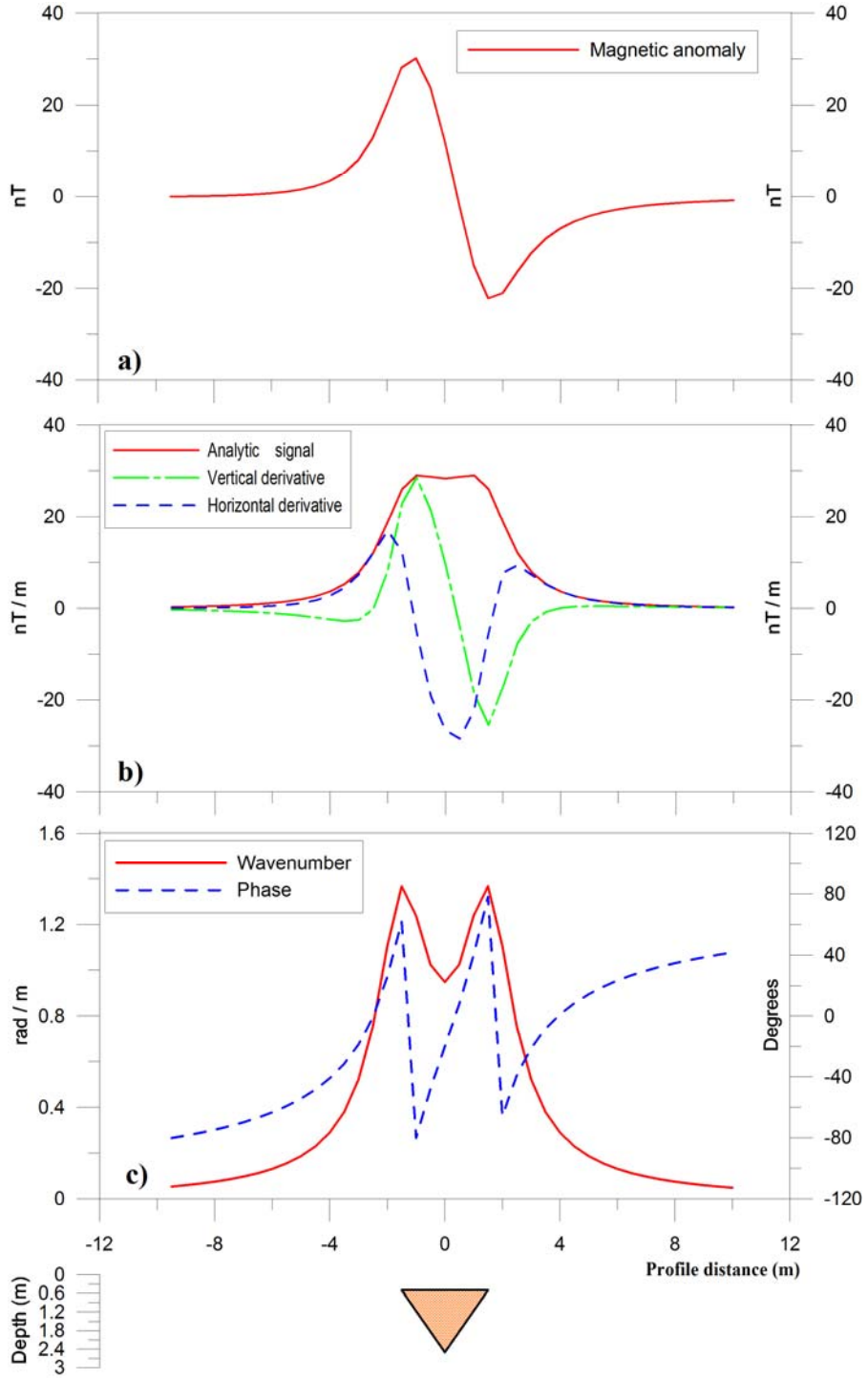

***Figure 6**: Same as Figure (4) for the triangular body of dimensions 3 m × 2 m (model c of Figure 3).*

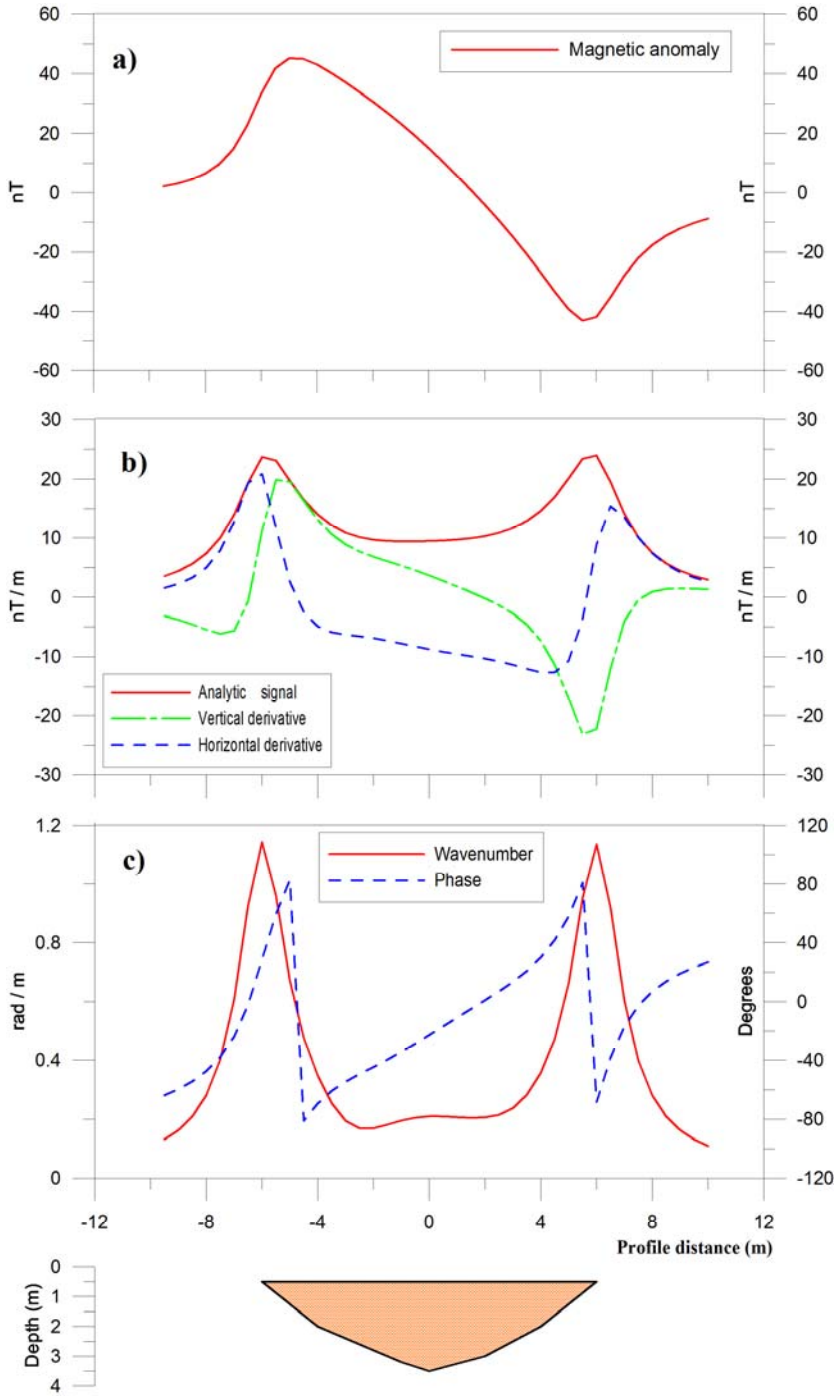

Figure 7*: Same as Figure 4 for the heptangular body of dimensions 12×3 (model d in Figure 3).*

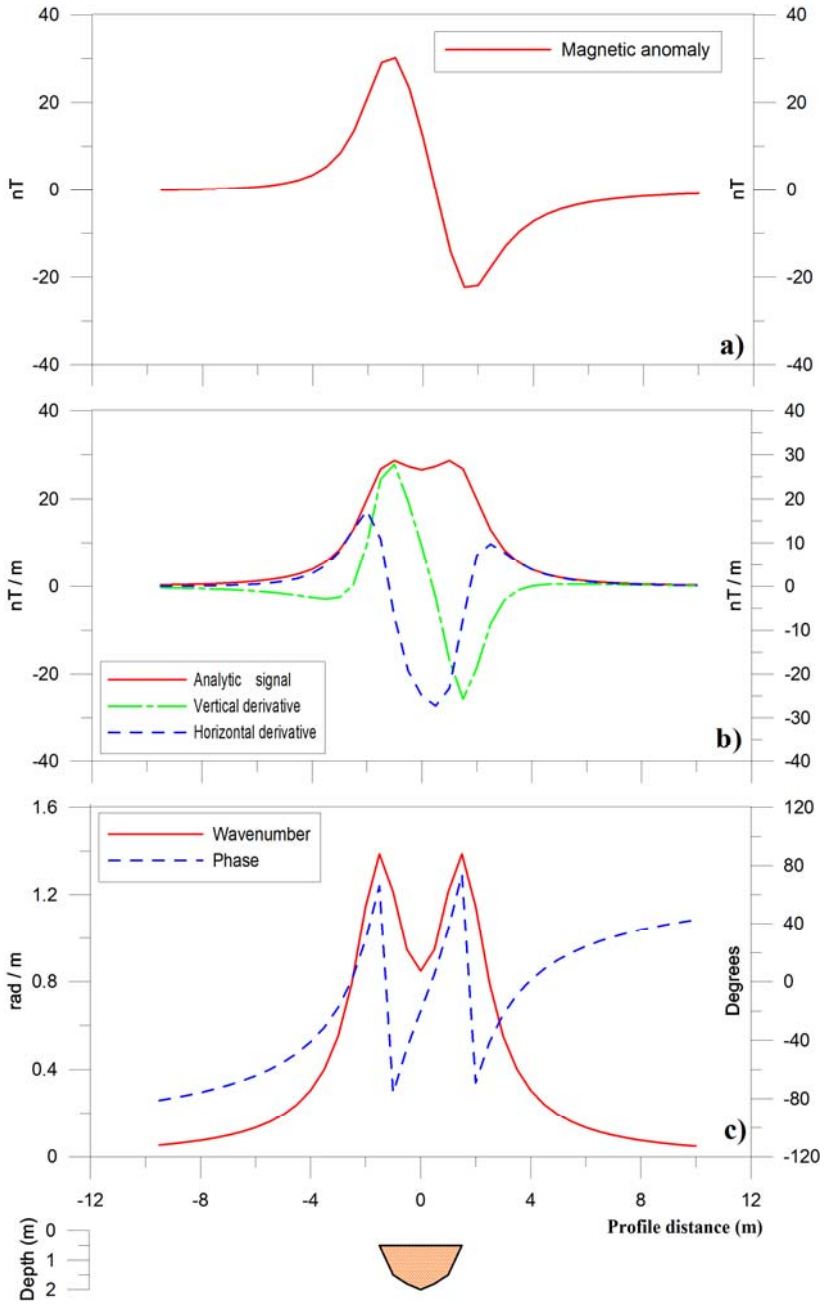

***Figure 8**: Same as Figure 4 for the heptangular body of dimensions 3×1.5 (model e in Figure 3).*

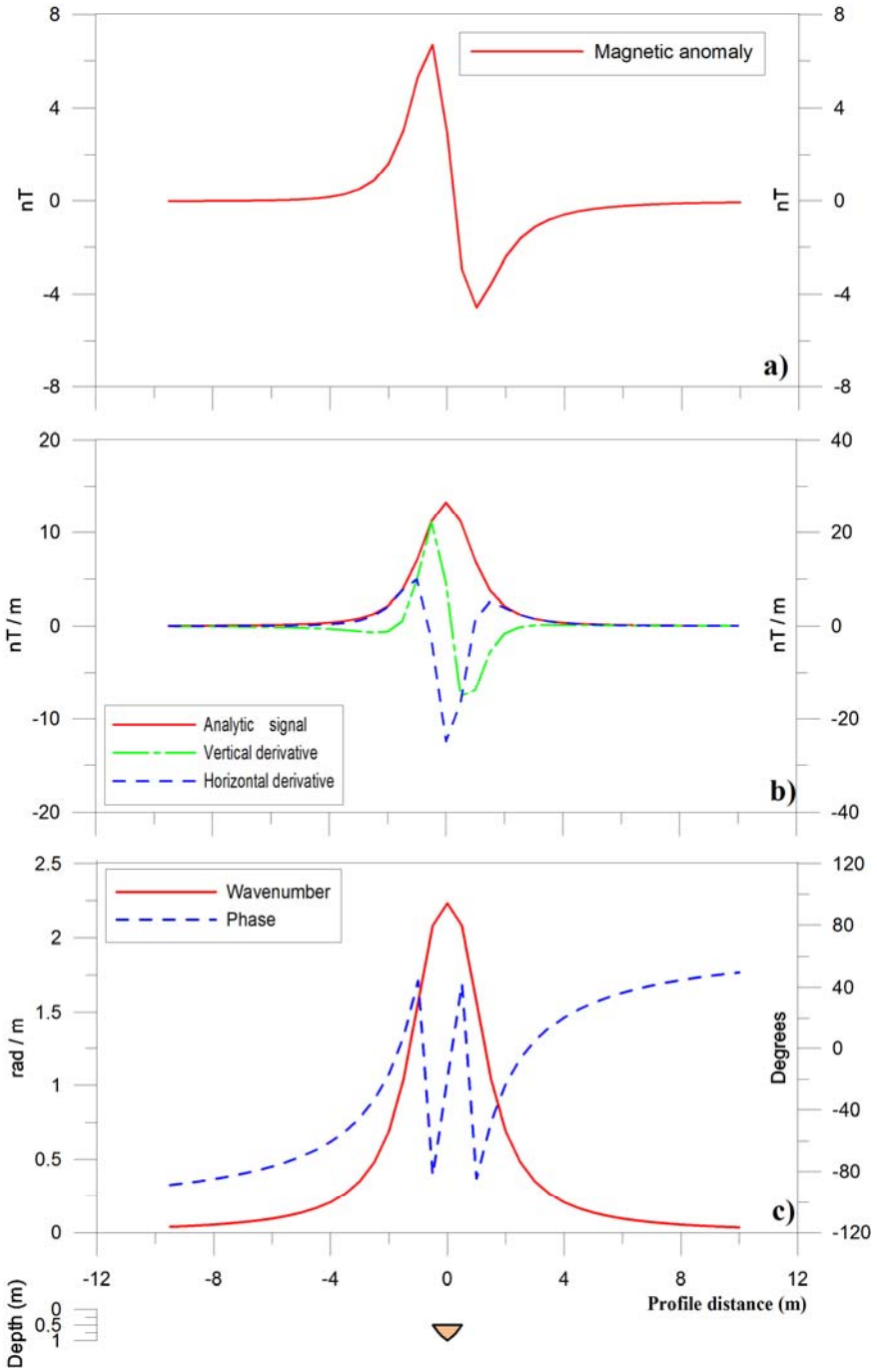

***Figure 9**: Same as Figure (4) for the heptangular body of dimensions 1×0.5 (model f in Figure 3).*

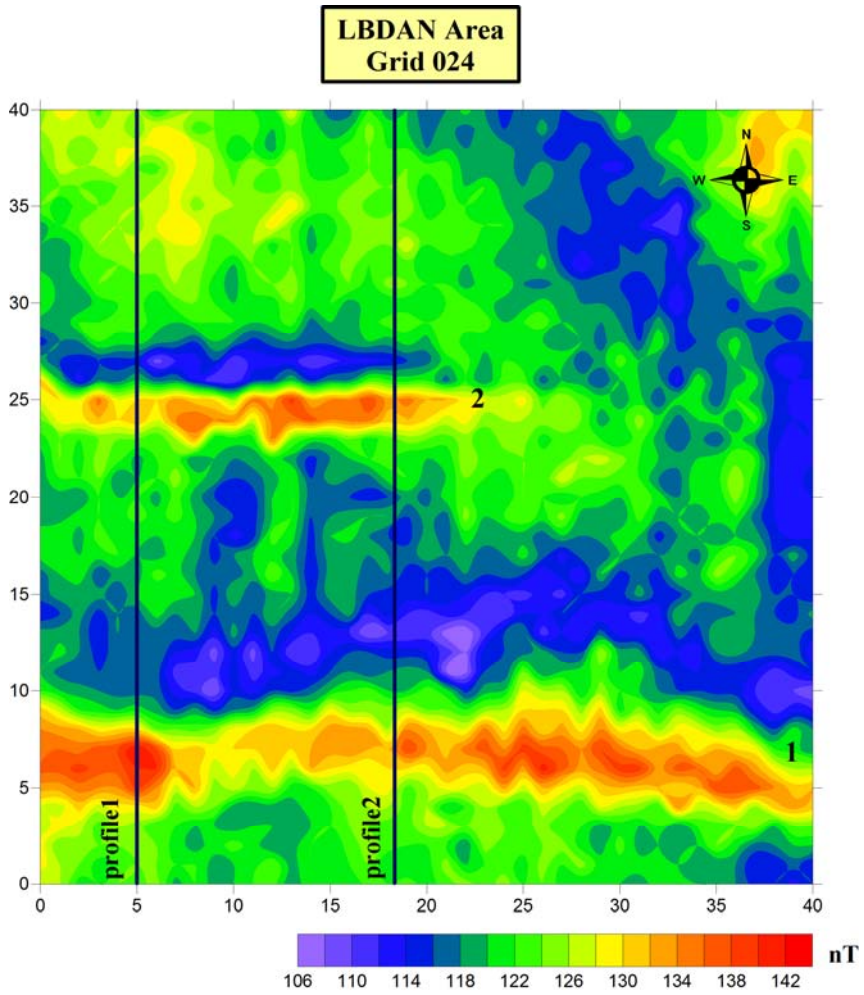

Figure 10: *Total magnetic filed distribution over a 40mX4m grid 024 extracted from the data taken during the investigation of the prehistoric site of Makrygialos, in Pieria (Region of Macedonia, Northern Greece) Tsokas et. all (1997). Two elongated anomalies are observed and denoted a 1 and 2. They comprise the response of two concealed prehistoric ditches. Also the two profiles, along which the multiple source complex attributes method was applied, can be seen.*

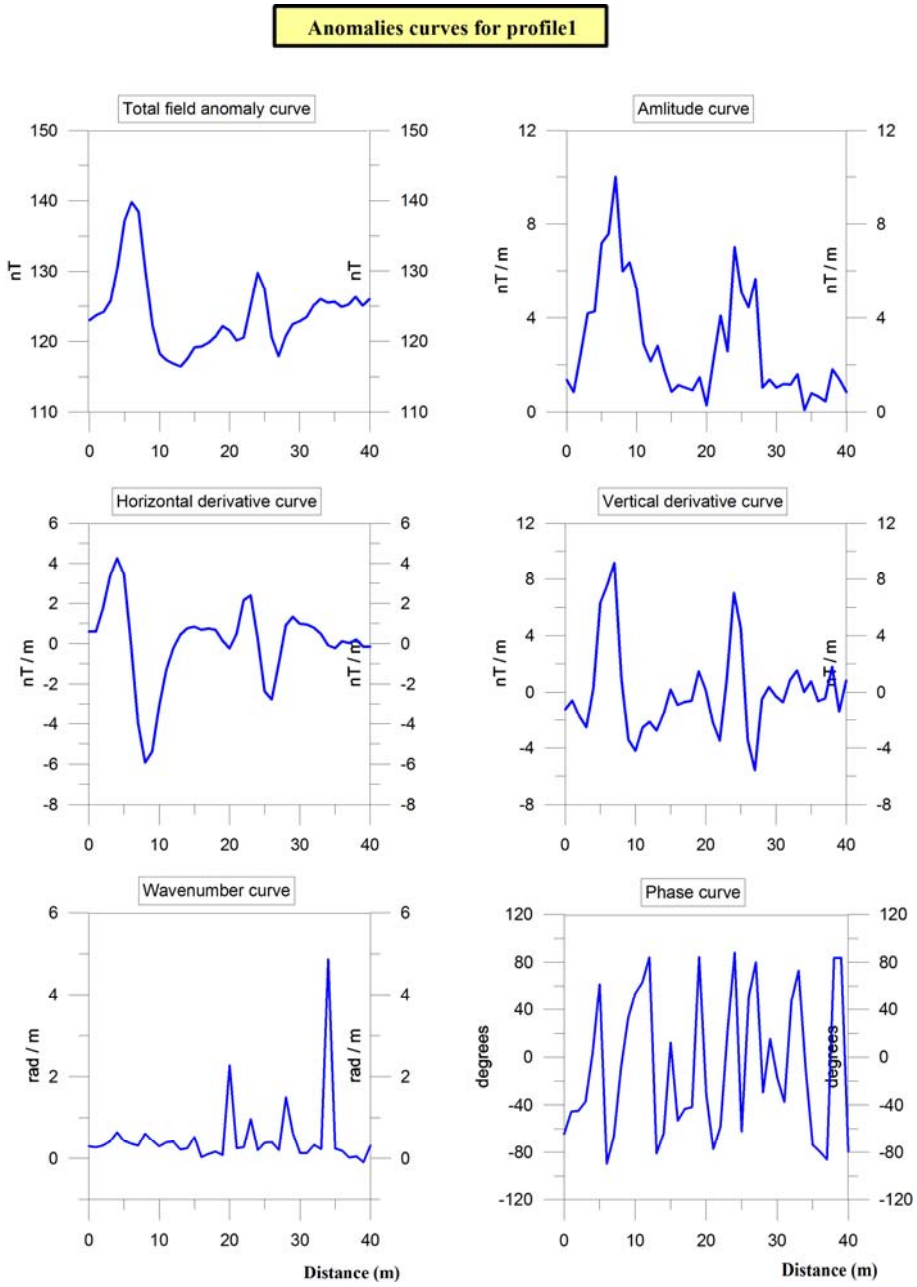

Figure 11: *Curves of the total field anomaly, amplitude, horizontal and vertical derivative, wavenumber and phase for the profile 1. Both the wavenumber and phase function appear noisy, while the amplitude function provides the exact location of the ditches.*

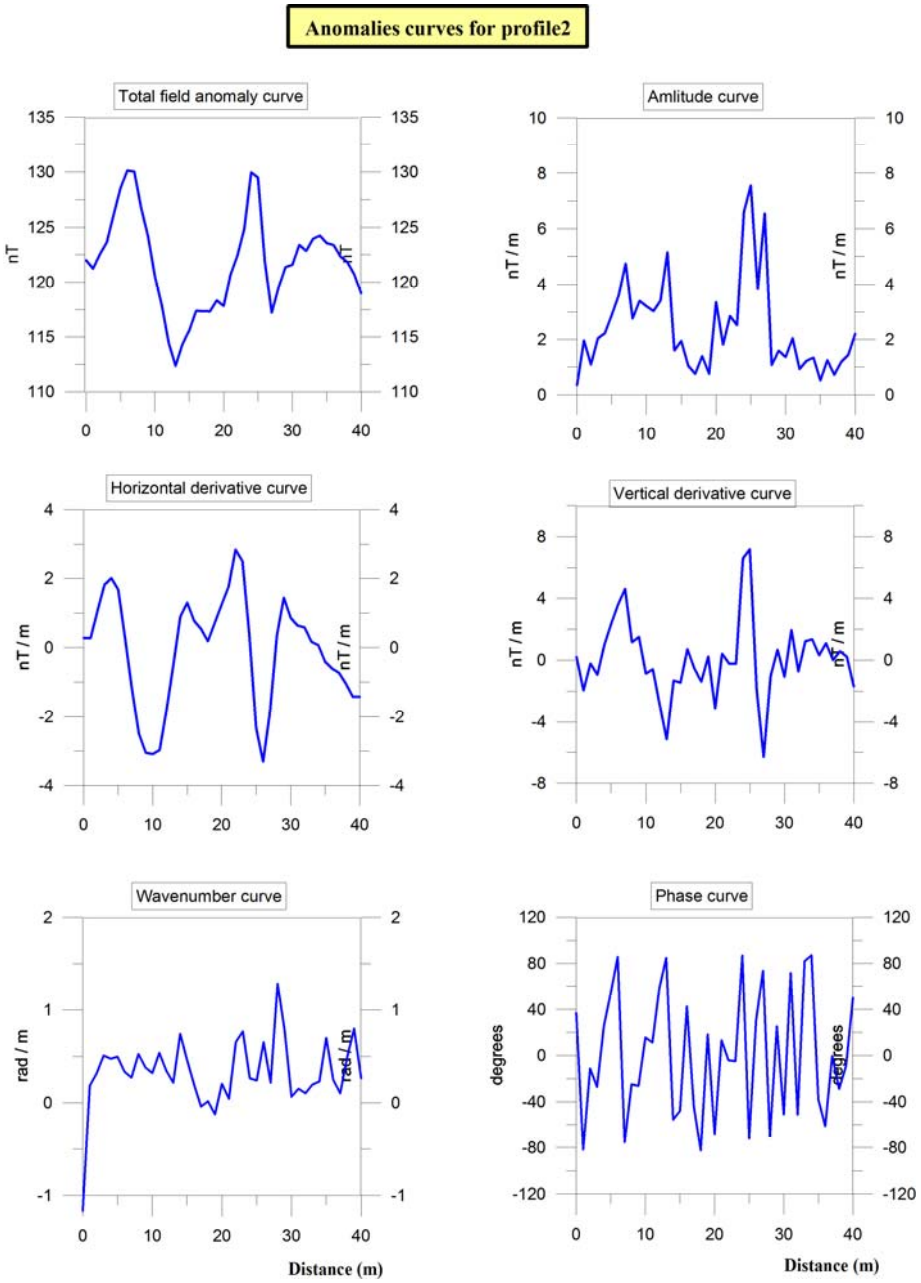

Figure 12: *Curves of the total field anomaly, amplitude, horizontal and vertical derivative, wavenumber and phase for the profile 2. Both the wavenumber and phase anomalies are obscured by noise while the amplitude function gives satisfactory result.*

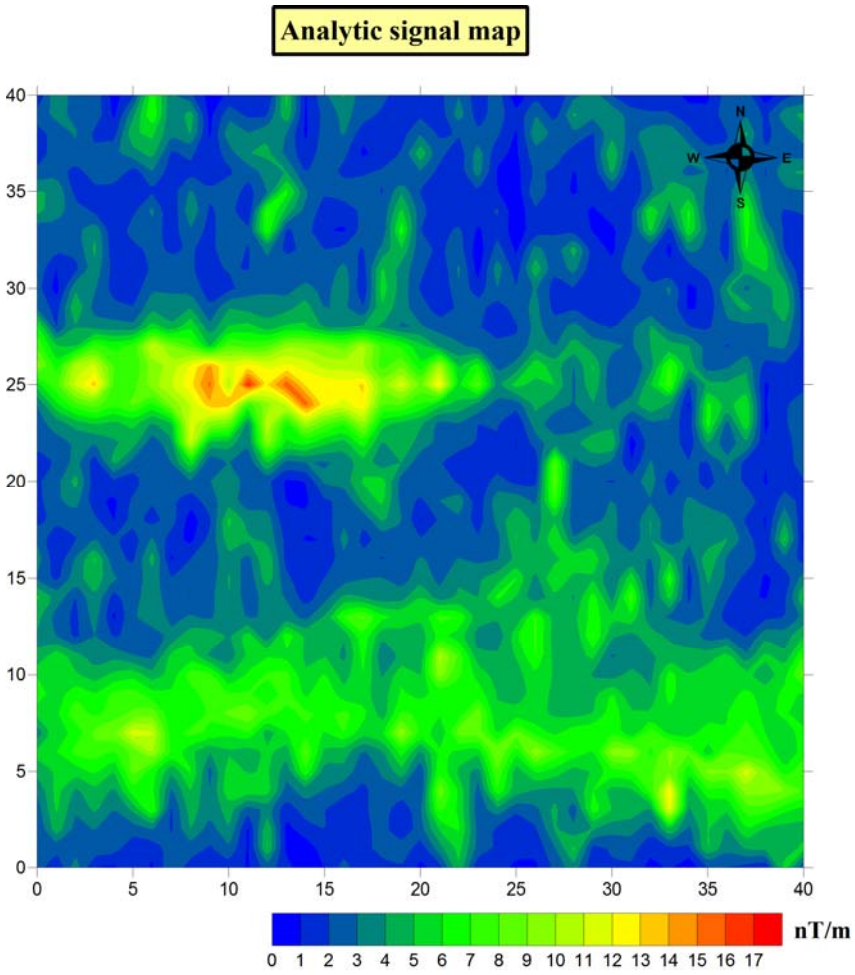

Figure 13: *Map of the amplitude function for grid 024. The positions and shapes of the two anomalies coincide with those in Figure 11 of the total field anomaly map.*